Journal of Mining and Environment (JME), Vol. 14, No. 4, 2023, 1343-1359

Shahrood University of Technology

Journal of Mining and Environment (JME)

Journal homepage: www.jme.shahroodut.ac.ir

Iranian Society of Mining Engineering (IRSME)

Identifying Corresponding Earthquake of Mobarak Abad Landslide, Northeast Tehran, Iran

Erfan Amini[1], Masoud Mojarab[2], and Hossein Memarian[1]*

1. School of Mining Engineering, College of Engineering, University of Tehran, Tehran, Iran
2. Bonyan Zamin Paydar Consulting Engineers, Tehran, Iran

Article Info

Received 7 July 2023
Received in Revised form 24 August 2023
Accepted 1 September 2023
Published online 1 September 2023

DOI: 10.22044/jme.2023.13339.2453

Keywords

Empirical equations
Landslide volume
Magnitude
Epicenter and hypocenter
Peak ground acceleration

Abstract

Landslides are defined as the downward movement of a portion of land materials under the direct influence of gravity. Landslides would get triggered by a wide spectrum of initiative factors such as earthquakes as a site effect of that event. In the vicinity of Tehran, significant historical earthquakes have occurred; therefore, tracing them could enhance the Tehran's historical earthquake catalogue, due to the reason Tehran is a metropolitan and capital of Iran. However, paleoseismology could not determine the magnitude and seismic characteristics of historical earthquakes. Mobarak Abad landslide is a large and historical landslide located on Haraz road, a vital artery connecting Tehran to the Mazandaran Province, and there are significant faults like Mosha, North Alborz, and Khazar in its neighborhood. Hence, it is probable that this landslide occurred due to the generation of dynamic force resulting from an earthquake. Therefore, in this study, the geometrical characteristics of the landslide were measured by field surveying. Then with the empirical equations proposed by various researchers, we estimated the landslide volume and the magnitude of the corresponding earthquake, respectively. In the following, the epicenter and hypocenter of all the historical earthquakes within 200 kilometers of the landslide were identified. Then we utilized some conditions such as Keefer's graphs, error value in epicenter location, and peak ground acceleration to omit earthquakes and identify the corresponding earthquake event. The results demonstrate that two earthquakes of 1830 AD and 855 AD with a maximum acceleration of 0.16g are more probable than the 743 AD earthquake.

1. Introduction

The downward movement and displacement of a portion of the slope materials is called a landslide [1]. Highland and Bobrowsky [2] define this natural hazard as the declination of a mass of rock, debris or earth downward a slope. Landslides are a type of mass wasting referring to any down-slope movement of rock and soil that occur under the direct influence of gravity force due to natural or human activities [3]. This phenomenon includes five modes of slope movement: falls, topples, slides, spreads, and flows [2]. A vast spectrum of factors are involved in triggering and creating a landslide, as well as they also can trigger other natural phenomena such as tsunamis [4]. We can mention slope angle, lithology, and structural geology of the area, undercutting the slope foot, buildings and traffic loads, storage of alluviums on the slope, earthquakes, vegetation cover and deforestation, water concentration due to rainfall, and increase in pore water pressure, laterization and deduction in cohesive strength, freezing and thawing, and volcanic activities [2,5,6]. Historically, earthquakes are known as one of the most influencing factors in landslide occurrence [1]. For instance, Jiuzhaigou earthquake induced over 5600 landslides [7], and Avaj earthquake triggered more than 550 landslides [8]. The earthquakes can cause slope instability and generate a landslide by a dynamic force; however, the mechanism and distribution of triggering a landslide remains an arguable task [9]. Since 373

✉ *Corresponding author: memarian@ut.ac.ir (H. Memarian)*

or 372 B.C., all earthquake-triggered landslides have been collected and recorded [10].

Landslides can also occur in residential areas located at hillsides or slopes of mountains. Depending on the volume of the displaced material, a landslide that occurs in such areas can result in fewer or higher casualties and economic losses. The scale of a landslide is determined by its morphology, which has a great impact on the stability of the deposit and hinders it from secondary movements [11]. In terms of casualties, landslides are the sixth deadliest natural disaster in the 20th century [12]. Table 1 shows the number of casualties due to the landslide occurrence in different continents from 1980 to 2000.

Table 1. Number of casualties due to landslide from 1980 to 2000 [12].

Continent	Casualties	Total population (millions)	Number of casualties per million people
North America	62	307	0.01
Central America	38250	174	10.47
South America	57365	351	7.78
Europe	535	795	0.03
Africa	612	860	0.03
South Asia	2596	1300	0.10
East and Southeast Asia	5125	2205	0.11
Central Asia	1958	80	0.17
Australia	119	33	0.17

Collection of slippery masses, reconstruction of residential houses, and road reconstruction or the creation of alternative routes, disruption of traffic, and reduction of tax revenues due to the decline in the value of neighboring lands are financial consequences and economic losses.

Iran is located in mountainous regions of the seismic belt of the Himalayan-Alpine [13]; therefore, most of the cities and villages in the country are always on the verge of suffering small to large earthquakes and simultaneously landslide events. Over the years, more than 5,000 landslides have been recorded in Iran, almost all of them were in mountainous areas. Figure 1 shows the distribution of landslides in Iran and their occurrence location related to major faults.

Seimareh landslide, the largest landslide globally, was recorded in Zagros folds around 9000 years ago in Iran. Seimareh landslide has a length of about 16 kilometers, a width of 6 kilometers, and a thickness of 0.4 kilometers with a volume of 38 cubic kilometers. The total landslide area is also approximately 200 square kilometers [15,16]. The generated energy from the landslide was so great that it caused rock layers to crumble and the slippery material to move 20 kilometers alongside the slope and anticline [16]. As a consequence of the Seimareh landslide, the Kashkan and Seimareh Rivers on the slopes of Kabirkuh Mountain were blocked, consequently; a form of natural dam was created, and the Seimareh Lake was born [16]. Generally, large-scale landslides, especially those blocking the river's route, are the most dangerous phenomena in mountain areas worldwide [17].

The city of Tehran is located in a high seismicity region with numerous historical earthquakes occurrence. Therefore, due to the reason that some earthquakes have side effects like triggering a landslide, recognizing the magnitude and seismic characteristics of historical earthquakes and consequently enhancing the historical earthquake catalogue is prominent. Many years ago, in the neighborhood of Tehran city around the Mobarak Abad village, a landslide occurred and the effects of this landslide are also observable. Mobarak Abad landslide continues to be active and every year the road passing through the landslide sinks a few centimeters downwards in the area. There are many faults near Mobarak Abad landslide such as Mosha, Caspian, Kandovan, and North Alborz. The existence of active faults and following that the high seismicity of this area can lead to earthquakes as the main cause of the landslide events.

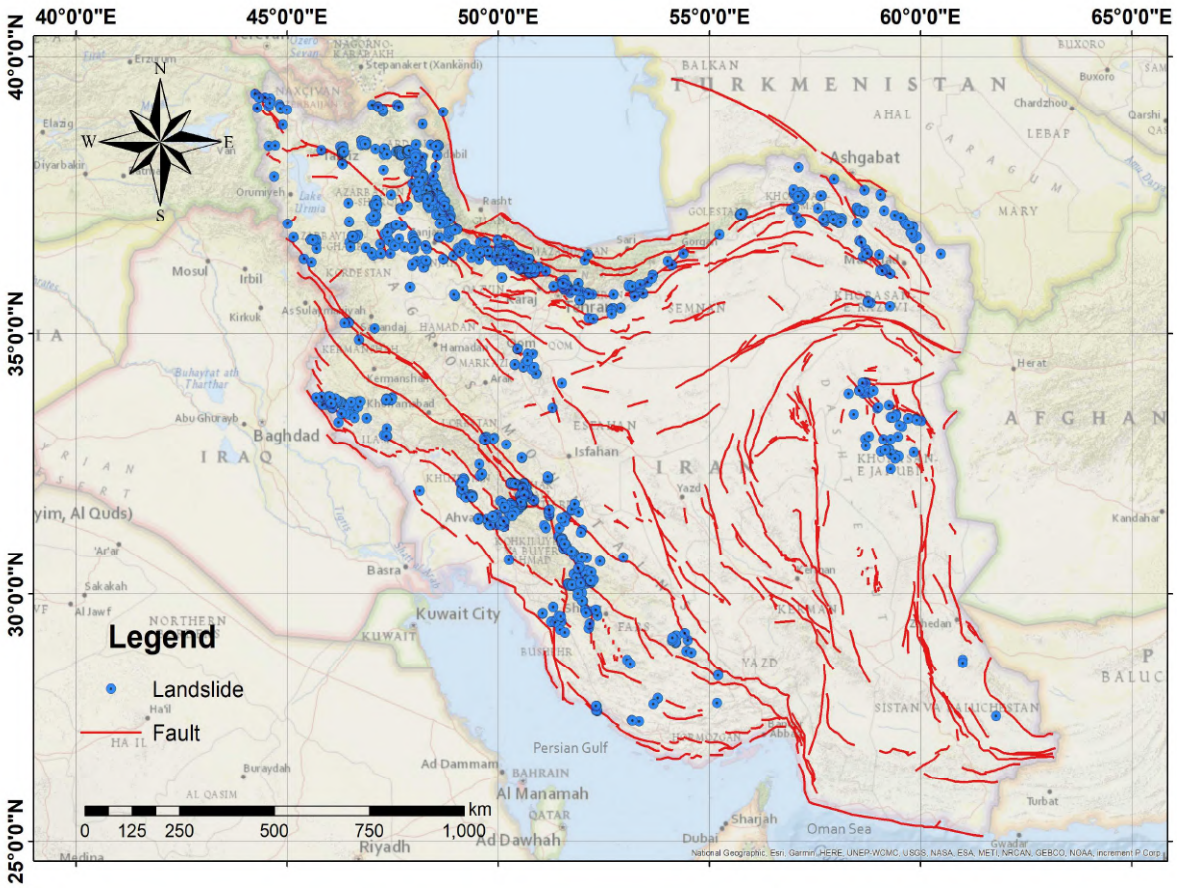

Figure 1. Distribution of landslides in Iran (modified from the map of "Major Active Faults of Iran" produced and published by Hessami *et al.* [14] and the International Institute of Earthquake Engineering (IIEES), respectively).

Various methods such as seismology, paleoseismology, archaeoseismology, and the use of morphological changes generated by historical earthquakes are used to identify those earthquakes when seismographic equipment was not adequate. However, due to the lack of sufficient evidence regarding the relationship between morphological changes and past earthquakes, this part of the study is usually deficient. However, in the present paper, as there is sufficient evidence such as historical reports, and morphological and tectonic evidence indicating the occurrence of a large-scale earthquake, the seismic characteristics and corresponding earthquake of the Mobarak Abad landslide were identified and documented by collecting all the historical earthquake events within 200 kilometers of the landslide, the relation between the magnitude of earthquake and geometry of Mobarak Abad landslide, and using the approach, which was presented by Keefer [1].

2. Regional setting of the studied area

2.1. Location and access road to Mobarak Abad landslide

The Mobarak Abad landslide is located in the central Alborz heights, between Abali and Mobarak Abad villages, on Haraz road, a critical corridor accessing Tehran to the Mazandaran Province, and 50 kilometers from Tehran the capital city of Iran, and one kilometer from Abali village. Indeed, the Mobarak Abad landslide is still active, and every year the road passing through the landslide is moving a few centimeters downwards in the area. The actual rate of displacement within the landslide is undefined. However, with different methods such as GPS*, SAR□ interferometry, and airborne Lidar□, we can evaluate the surface displacement of the Mobarak Abad landslide. Also a small amount of concreting has been done on the

* Global Positioning System

□ Synthetic Aperture Radar

□ Light Detection and Ranging

heel of the landslide, to prevent the downward movement of the landslide. As Figure 2 shows, Haraz road divides the landslide into two parts. Figure 2(a) shows the actual and airborne images of the landslide in Haraz road, and Figure 2(b) also shows the 3D image of the landslide prepared by the topography map and level contours of the area. In all the images, the landslide boundary is marked by using dashed lines. The existence of active faults such as Mosha, Caspian, Kandovan, and North Alborz faults and further induced high seismicity of this area could make earthquakes the dominant cause of the landslide.

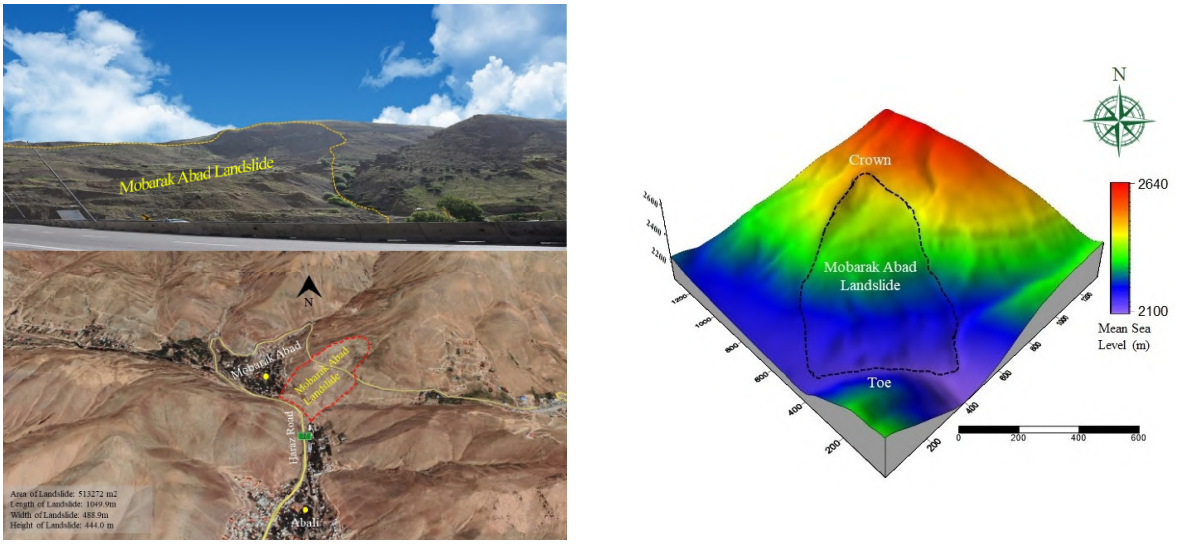

(a) **(b)**

Figure 2. (a) Location of Mobarak Abad landslide and (b) 3D picture of the landslide.

We also surveyed the Mobarak Abad landslide, and recorded the coordination of different parts of it with GPS. Figure 3 demonstrates the Mobarak Abad landslide and the crack on its crown. The newest residential districts of Mobarak Abad villages spread in southwestern parts of the landslide.

As stated above, the Mobarak Abad landslide indeed continues to be active, which could be induced by a variety of driving forces, e.g. the road passing through the landslide and the traffic load generated by the cars, rainfall, occurrence of microseismic events or washing away of the landslide toe by Jajrood River. Its downward movement causes successive damages to the asphalt of the Haraz road insofar as the thickness of the asphalt at some points reaches almost 20 centimeters for compensating the diminished asphalt (Figure 4).

2.2. Geology and structural geology

Figure 5 illustrates the geology map of the Mobarak Abad landslide (1:100,000) provided by the Geological Survey and Mineral Explorations of Iran (GSI). The studied area is approximately located in the longitude range of 51°57’15” N to 51°59’00” N and latitude range of 35°46’00” E to 35°47’20” E. Based on the geology map of the area, the rock units belong to Karaj, Ziarat, Fajan, Elika, Mobarak, Jeirud, Mila, Lalun, Zagun, Barat, and Soltanieh formations. Also the rock units are composed of a wide variety of geological eras, from the Quaternary period Holocene epoch in the Cenozoic era to the Late Neoproterozoic era and Igneous rocks outcrops like T^{gb} unit.

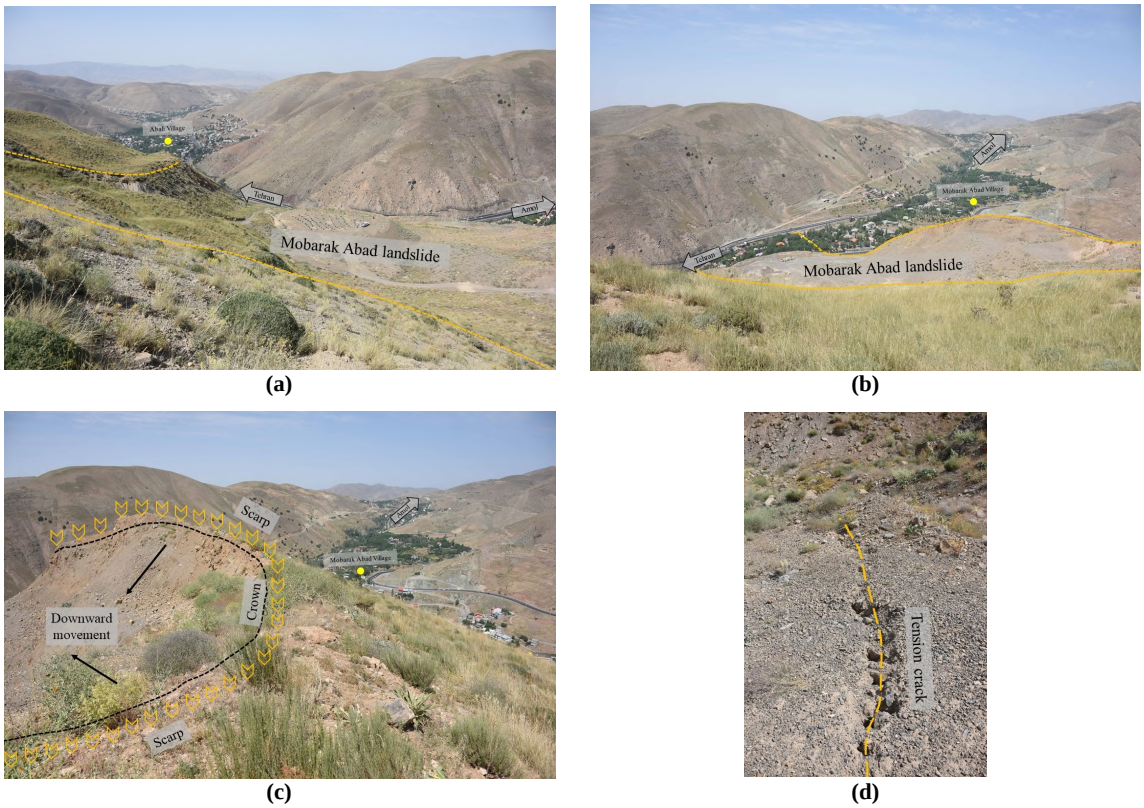

Figure 3. Mobarak Abad landslide (a) Northwest view, (b) Northeast view, (c) scarp and crown, and (d) tension crack on its crown.

Figure 4. Repaired asphalt in Haraz road passing through the landslide.

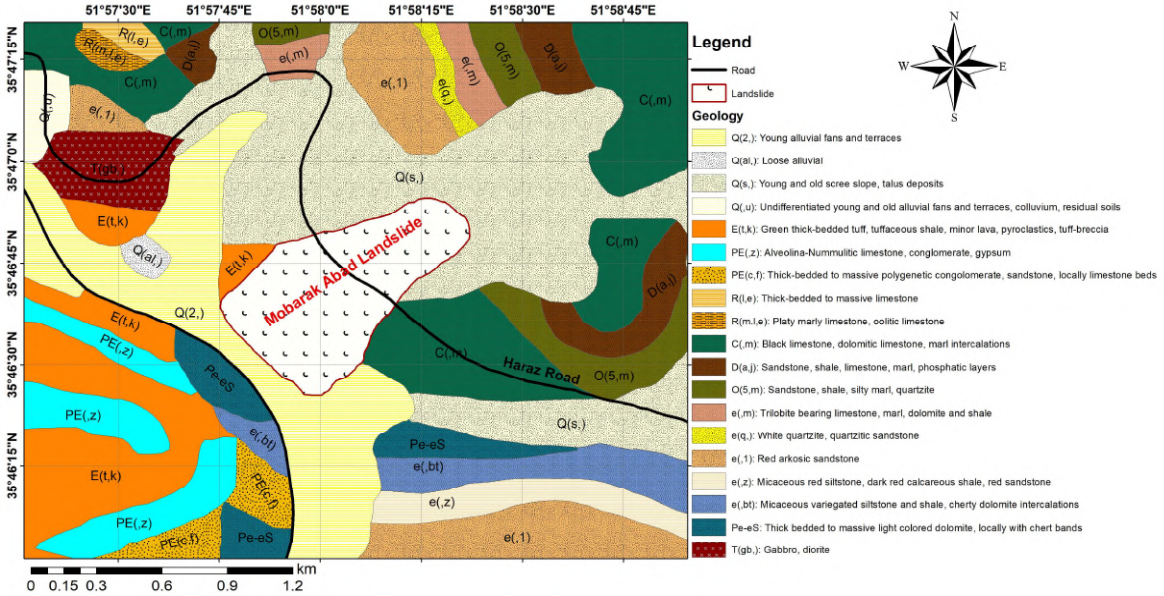

Figure 5. Geology map of the area (modified from the geology map of "East of Tehran" produced and published by Sahbai *et al*. [18] and Geological Survey and Mineral Exploration of Iran (GSI), respectively).

Mobarak Abad landslide has occurred in alluvium above the strong Carboniferous limestone of the Mobarak formation and the marly-limestone of the Permian Nesen formation. The thickness of this limestone mass in the landslide section reaches more than 400 meters [19]. The most critical tectonic structures in the vicinity of Mobarak Abad landslide are active faults such as Mosha, Khazar, North Alborz, and North Tehran. Figure 6 shows the location of active faults up to a radius of 200 kilometers from the center of the landslide.

3. Materials and methods

3.1. Volume of landslide

Calculating the Mobarak Abad landslide volume is a significant part of the current study; in the following, we can determine the magnitude of the corresponding earthquake through the estimated volume. In addition, the landslide volume is an essential factor for stability analysis and risk assessment [20]. It is difficult to calculate the volume due to the three-dimensional nature of the landslide and the exact shapes and locations of rupture zones since the Mobarak Abad landslide is a historical event starting at some point earlier, we could not calculate the volume of such an event simply by mapping techniques like the UAV* imagery method (which was conducted by Valkaniotis *et al*. [21]). Nevertheless, as mentioned in Eq. 1, the following relationship is established between the volume and landslide area in all the cases [22].

$$V_l = \varepsilon A_l^{\alpha} \quad (1)$$

Based on the above equation, many researchers have developed different formulas to interconnect landslide area to volume. Some other equations (Eq. 2) are slightly more comprehensive and relate length, width, height, slope angle, and peak ground acceleration to volume [23].

$$V = f(A, L, W, H, Lith, Slp, PGA) \quad (2)$$

where A is landslide area, L is the landslide length, W is the landslide width, H is the landslide height, Lith is the petrology of landslide, Slp is the slope angle, and PGA is the peak ground acceleration at the landslide.

Based on the available parameters for the Mobarak Abad landslide, the below method is followed to calculate the landslide volume:

1. In this stage, the length, width, height, and area of the landslide were calculated by field surveying and recording the coordinates of the landslide boundaries and plotting them in ArcMap software. Table 2 shows the geometry characteristics of the Mobarak Abad landslide.

* Unmanned Aerial Vehicles

Table 2. Geometry characteristics of Mobarak Abad landslide.

Parameters	Value
Area of landslide (A_L), m^2	513272
Length (L), m	1049.9
Width (W), m	488.9
Height (H), m	444

2. For calculating the landslide volume, we examined forty-two different equations relating the geometry of the landslide to the volume. However, some of them have some limitations to use. For instance, the equation $V_L = 1.0359A_L^{0.880}$ presented by Martin *et al.* [24], only can be used for the landslides whose area is between 2×10^2 m^2 to 5.2×10^4 m^2, whereas the area of the Mobarak Abad landslide is not within the desired range. For this reason, the equations whose conditions do not match the geometry characteristics of the Mobarak Abad landslide were omitted, and only 29 equations remain. Finally, as shown in Table 3, the volume of the Mobarak Abad landslide based on its geometry characteristics was calculated by the remaining equations.

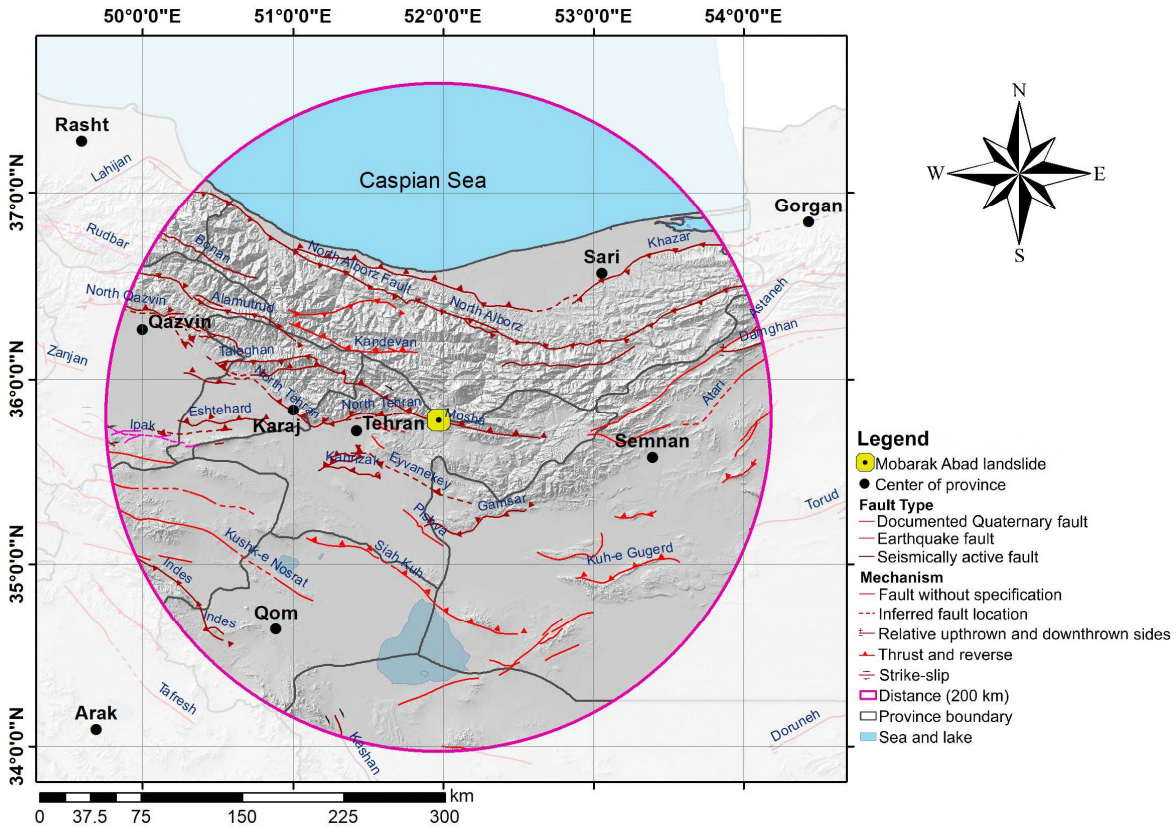

Figure 6. Location of the active faults around the Mobarak Abad landslide (modified from the map of "Major Active Faults of Iran" produced and published by Hessami *et al.* [14] and the International Institute of Earthquake Engineering (IIEES), respectively).

Table 3. Calculated volumes for Mobarak Abad landslide.

	Equation	Min A_L (m^2)	Max A_L (m^2)	Volume (m^3)	Source
1	$V_L = 0.242A_L^{1.250}$	2×10^5	6×10^7	3324679.9	Abele [25]
2	$V_L = 1.55A_L^{1.183}$	2×10^5	6×10^7	8824149.9	Abele [25]
3	$V_L = 0.769A_L^{1.250}$	4×10^4	3.9×10^6	10564788.5	Whitehouse [26]
4	$V_L = 12.273A_L^{1.049}$	3×10^5	3.9×10^{10}	11997902.8	Haflidason [27]
5	$V_L = 4.655A_L^{1.292}$	5×10^5	2×10^8	111093525.7	Ten Brink *et al.* [28]
6	$V_L = 0.263A_L^{1.292}$	5×10^{-1} (km^2)	2×10^2 (km^2)	111102751.2	Ten Brink *et al.* [28]
7	$V_L = 0.0844A_L^{1.4324}$	10	10^9	12759813.0	Guzzetti *et al.* [29]
8	$V_L = 0.074A_L^{1.450}$	2	10^9	14100538.6	Guzzetti *et al.* [22]
9	$V_L = 3.4573A_L^{1.2053}$; A_L ($\times 10^4$); V_L ($\times 10^4$)	_____	_____	3983079.7	Fan *et al.* [30]
10	$V_L = 0.0009H^2 + 0.0305H + 5.9052$; V_L ($\times 10^4$)	_____	_____	1968696.0	Fan *et al.* [30]
11	$V_L = 0.0974A_L^{1.176}$	1.23×10^2	1.085×10^6	505740.5	Omidvar and Kavian [31]
12	$V_L = 0.4763A_L^{1.244}$	_____	_____	6047180.9	Hadian-Amri *et al.* [32]
13	$V_L = 0.4261A_L^{1.2572}$	_____	_____	6435177.1	Hadian-Amri *et al.* [32]
14	$V_L = 2\times10^{-05}A_L^2 + 12.691A_L - 53720$	_____	_____	11729177.9	Hadian-Amri *et al.* [32]
15	$V_L = 2.482A_L^{1.024}$	_____	_____	1746617.0	Amirahmadi *et al.* [33]
16	$V_L = 1.315A_L^{1.2018}$	_____	_____	9585647.8	Xu *et al*. [23]
17	$V_L = 1.0897A_L^{1.2146}$	_____	_____	9399291.7	Xu *et al*. [23]
18	$V_L = 1.3147A_L^{1.2085}$	_____	_____	10466023.5	Xu *et al*. [23]
19	$V_L = 3.924L^{1.953}$	_____	_____	3118867.9	Xu *et al*. [23]
20	$V_L = 107.05L^{1.3467}$	_____	_____	1253554.4	Xu *et al*. [23]
21	$V_L = 30.303W^{2.203}$	_____	_____	25458376.3	Xu *et al*. [23]
22	$V_L = 648.86W^{1.3119}$	_____	_____	2188440.8	Xu *et al*. [23]
23	$V_L = 5.811H^{1.949}$	_____	_____	839460.5	Xu *et al*. [23]
24	$V_L = 857.29H^{1.018}$	_____	_____	424779.7	Xu *et al*. [23]
25	$\ln(V_L) = 0.0859 + 1.2146\ln(A_L)$	_____	_____	9399268.6	Xu *et al*. [23]
26	$\ln(V_L) = 0.0127 + 1.0524\ln(A_L) + 0.3151\ln(H)$	_____	_____	7067660.8	Xu *et al*. [23]
27	$\ln(V_L) = 0.3527 + 0.612\ln(L) + 1.2108\ln(W) + 0.582\ln(H)$	_____	_____	6294893.9	Xu *et al*. [23]
28	$V_L = 0.9105\times A_L^{1.1693} \times H^{0.1348}$	_____	_____	9845926.6	Xu *et al*. [23]
29	$V_L = 0.8919 \times L^{1.0493} \times W^{1.2188} \times H^{0.2223}$	_____	_____	9694365.5	Xu *et al*. [23]

3. As shown in Table 3, the calculated values are very variable, but some are close to each other; therefore, out-of-range data should be eliminated. As shown in Figure 7(a), among these 29 values, only six were out of range and were deleted (three values from the top and three values from the bottom). After deleting these eccentric values, the remaining values' Q-Q plot was plotted again in Figure 7(b). The presented graph showed a good trend and was S-shaped. Due to the logarithmic relation that governs the landslide volume and magnitude of the corresponding earthquake (Section 3.2), no change was detected in the value of the determined magnitude by deleting more volume data.

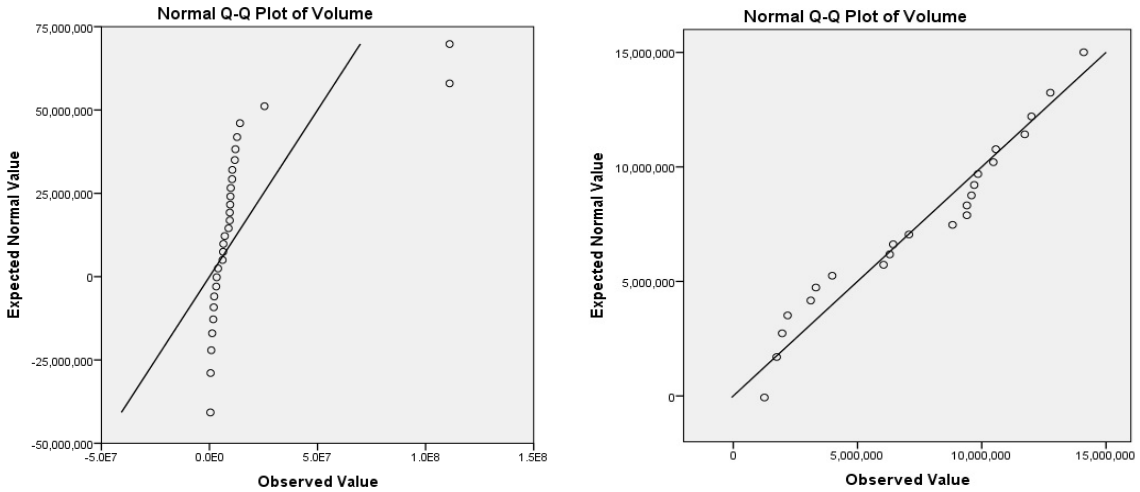

(a). Q-Q plot of raw values **(b). Q-Q plot after deleting out-of-range values**

Figure 7. Q-Q plot of the (a) raw values and (b) after omitting out-of-range values.

4. At last, the volume of landslide could be estimated by averaging the remaining values. Nevertheless, since the data are diverse, it is better to report the landslide volume in a range between Mean-ST.D to Mean+ST.D, where the Mean is the average and ST.D is the standard deviation of the values, respectively. Therefore, the standard deviation of those values was calculated. The average and standard deviation of the Table 3 values are 7469380.1 and 3907815.4 cubic meters, respectively. Based on the proposed equation, the landslide volume can vary from 3561564.7 to 11377195.5 cubic meters.

3.2. Magnitude of corresponding earthquake

After calculating the volume, we considered all the equations relating the volume or area of the landslide to the corresponding earthquake's magnitude (M). Some equations also relate the landslide volume to seismic moment (M_o) and seismic moment (M_o) to magnitude. In this form of the equation, first, the value of the seismic moment was calculated from 3 different equations proposed by Keefer and Wilson [34] and Keefer [35], and later the landslide volume was estimated from the previous section. With the Hanks and Kanamori [36] equation, which relates the seismic moment to magnitude, the magnitude of the corresponding earthquake was evaluated for these three seismic moment values.

For each equation, the magnitude was calculated. Similar to volume, since the calculated values are different, estimating the magnitude of corresponding earthquake as a range in the form of Mean ± ST.D is accurate. Table 4 shows the calculated magnitudes by the equations relating the volume and area of the landslide to the earthquake's magnitude. It also should be noted that we used the averaged value of the landslide volume calculated from the previous section to determine the magnitude.

After calculating the magnitudes, the mean and standard deviation of the values were 6.3 and 0.9, respectively. Therefore, based on the above equation, the magnitude of the corresponding earthquake varies from 5.4 to 7.2.

4. Results and Discussion

4.1. Magnitude of historical earthquakes

To identify the corresponding earthquake of the Mobarak Abad landslide, all the historical earthquakes (earthquakes that occurred before 1900) occurred within a radius of 200 kilometers from the landslide, with three catalogs of Ambraseys and Melville [44], and Berberian [45,46] were considered and only the earthquakes with the magnitude in our estimated range were considered. As shown in Figure 8, only 28 historical earthquake events are within a radius of 200 kilometers from the Mobarak Abad landslide, and 24 of them have a magnitude between 5.4 and 7.2. Just four earthquakes have a magnitude out of this range. In Figure 8, also mesoseismal area of the earthquake events and its occurrence date are shown.

Table 4. Calculate the magnitude of the corresponding earthquake.

Equation	Condition	Calculated magnitude (M)	Source
$\text{Log } M_o = 1.5M + 16.05$	_____	6.6	Hanks and Kanamori [36]
$\text{Log } M_o = 1.5M + 16.05$	_____	6.5	Hanks and Kanamori [36]
$\text{Log } M_o = 1.5M + 16.05$	_____	6.5	Hanks and Kanamori [36]
$\text{Log } V = 1.44M - 2.34$; V ($m^3$)	_____	6.4	Keefer and Wilson [34]
$\text{Log } V = 1.45M - 2.5$; V ($m^3$)	$5.3 \leq M \leq 8.6$	6.5	Keefer [35]
$\text{Log } A = 0.96 (\pm 0.16)M - 3.7 (\pm 1.1)$; A ($km^2$)	_____	3.6	Hancox *et al.* [37,38]
$\text{Log } V_{LT} = 1.42M - 11.26 (\pm 0.52)$; V_{LT} (km^3)	_____	6.4	Malamud *et al.* [39]
$\text{Log } A_{Lmax} = 0.91M - 6.85 (\pm 0.33)$; A_{Lmax} (km^2)	_____	7.2	Malamud *et al.* [39]
$\text{Log } A_{LT} = 1.27M - 7.96 (\pm 0.46)$; A_{LT} (km^2)	_____	6.0	Malamud *et al.* [39]
$V_{LT} = 10^{-11.26 \pm 0.52} \times 10^{1.42M}$; V_{LT} (km^3)	_____	6.4	Malamud *et al.* [39]
$\text{Log } V_{Lmax} = 1.36M - 11.58 (\pm 0.49)$; V_{Lmax} (km^3)	$M \geq 4.3$	7.0	Nepop and Agatova [40]
$\text{Log } V_{LT} = 1.24M - 11.26 (\pm 0.52)$; V_{LT} (km^3)	$M \geq 4.3$	7.4	Nepop and Agatova [40]
$\text{Log } V_{LT} = 1.39M - 10.95$; V_{LT} (km^3)	$5.3 \leq M \leq 8.6$	6.3	Agatova and Nepop [41]
$A_{LT} = 9 \times 10^{-7\exp(2.4585M)}$	_____	5.4	Xu *et al.* [42]
$M = 0.78\text{Log } V_{Lmax} + 8.34$; V_{Lmax} (km^3)	$4.9 \leq M \leq 8.1$	6.7	Nepop and Agatova [43]
Equation	**Seismic Moment (dyn-cm)**		**Source**
$\text{Log } V = \text{Log } M_o - 19.1 (\pm 0.93)$; V ($m^3$)	940339242485282000000000000		Keefer and Wilson [34]
$\text{Log } V = 0.95\text{Log } M_o - 17.7$; V ($m^3$)	735555296294712000000000000		Keefer [35]
$\text{Log } V = \text{Log } M_o - 18.9$; V ($m^3$)	593313951349027000000000000		Keefer [35]

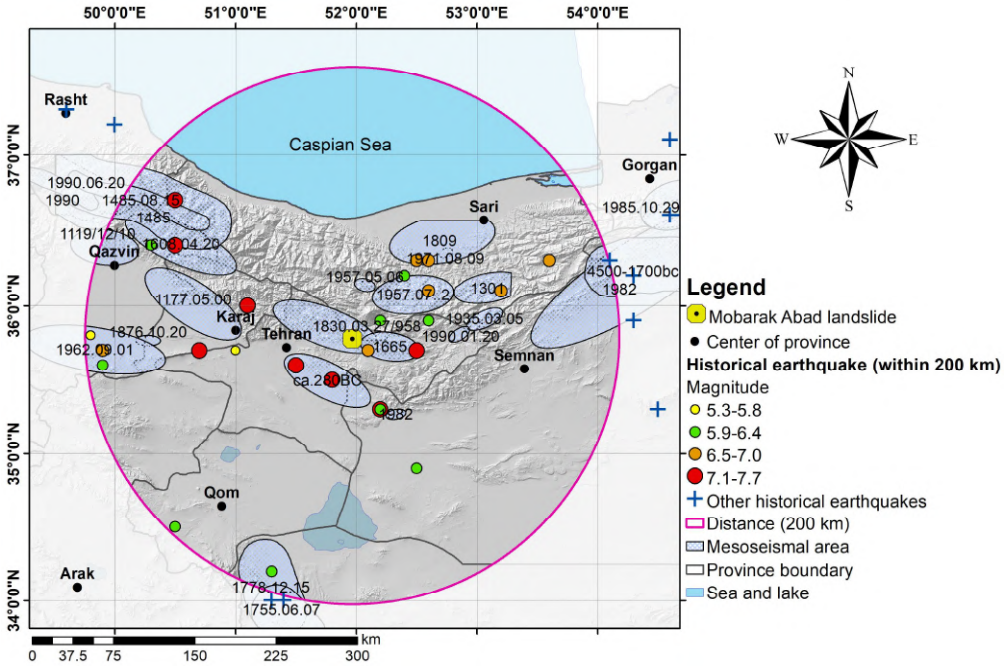

Figure 8. Historical earthquakes at a distance of 200 kilometers from the landslide.

Twenty-four earthquakes can be considered as the corresponding earthquake of the Mobarak Abad landslide. Therefore, more conditions are needed to eliminate more earthquakes and finally come up with a single earthquake and introduce this earthquake as the corresponding earthquake that triggered the Mobarak Abad landslide.

4.2. Epicenter and hypocenter distance from landslide

Figure 9 and Figure 10, presented by Keefer [1], illustrate the relation between the magnitude of a hypothetical earthquake and the maximum epicenter and hypocenter distance from an induced landslide. In cases where the focal point of the

earthquake is considered a point instead of the fault line, then the hypocenter distance is equal to the fault rupture zone. In Keefer's research work, the graphs were presented for three different types of landslides: (1) disrupted slides and falls: rock falls, rock slides, rock avalanches, soil falls, disrupted soil slides, and soil avalanches; (2) coherent slides: rock slumps, rock block slides, soil slumps, soil block slides, and slow earth flows; and (3) lateral spreads and flows: lateral soil spreads, rapid soil flows, and subaqueous landslides. The Mobarak Abad landslide is categorized as coherent slides (Graph B in Figure 9 and Figure 10).

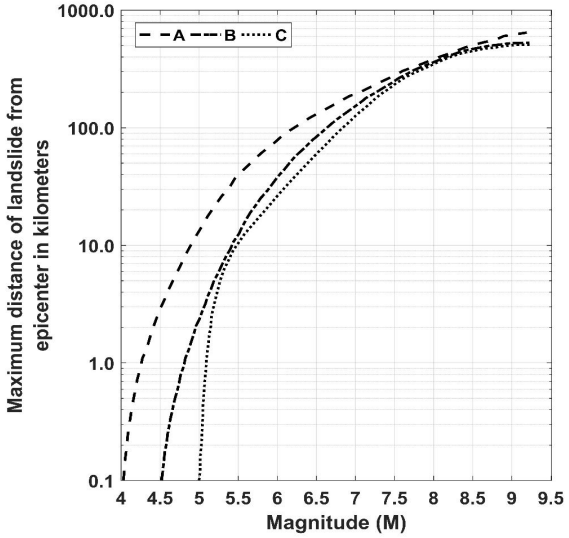

Figure 9. Maximum distance from epicenter to (a) disrupted slide or fall, (b) coherent slide, and (c) lateral spread or flow for earthquakes of different magnitudes [1].

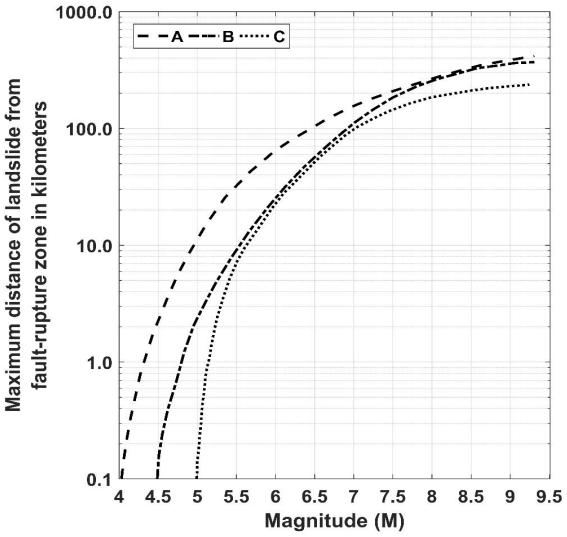

Figure 10. Maximum distance from fault-rupture zone to (a) disrupted slide or fall, (b) coherent slide, and (c) lateral spread or flow for earthquakes of different magnitudes [1].

The earthquake will be deleted if the values of the epicenter and hypocenter are more than the values presented in the graphs. To find the epicenter distance, we need to measure the distance between the earthquake and the landslide location. Calculating the hypocenter distance is not as simple as the epicenter distance. The studied earthquakes are historical; therefore, their occurrence depth, and consequently, the hypocenter are unknown. The occurrence depth of all the earthquakes that occurred in the Alborz zone after 1900 was extracted by Shahvar *et al*. [47] catalog is shown in Figure 11. By observing all of these depths, we found out that the value of 10 kilometers was more repetitive than other depths, and we chose that as the reference depth.

Finally, ten earthquakes were eliminated by the epicenter graph and seven by the hypocenter graph, respectively.

4.3. Error in epicenter location

For now, twenty-one historical earthquake events within a radius of 200 kilometers from the Mobarak Abad landslide have been eliminated, but there are still seven earthquake events that can be considered as the corresponding earthquake for the Mobarak Abad landslide occurrence.

The epicenter locations are not accurate, so that by using the publication No. 626 (Guideline for Seismic Hazard Analysis) of Iran, the maximum amount of epicenter location error for each timespan in every magnitude value was applied for the remaining earthquakes (Table 5). The Keefer [1] graphs were used again, and more historical earthquake events were removed. Lastly, we identified three corresponding earthquake events in 743 AD, 855 AD, and 1830 AD with the magnitude of 7.2, 7.1, and 7.1, respectively. The interesting point about these three remaining earthquakes is that their epicenter distance to the landslide is almost the same and near each other.

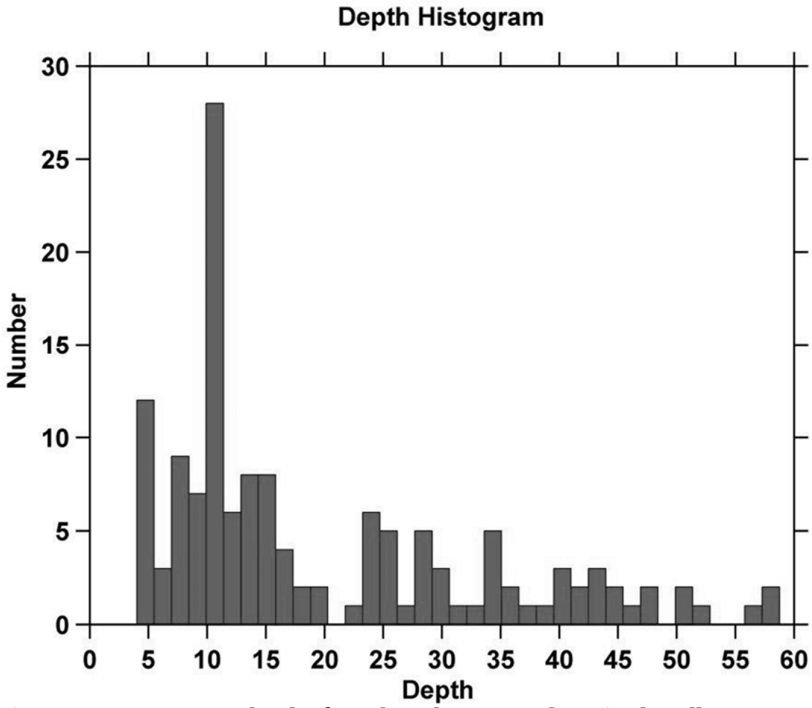

Figure 11. Occurrence depth of earthquakes came about in the Alborz zone.

Table 5. Error value in epicenter location for each magnitude value [48].

Time	M				
	> 7	6-7	5-6	4-5	3-4
< 1800	30-50	35-55	50-75	-	-
1800-1918	20-40	25-45	30-50	50-70	-
1918-1964	12	18	-	-	-
1964-1980	5.5	5.4	6.5	9.5	-
> 1980	3.5	4	4	8.5	13.5

4.4. Peak ground acceleration

To identify the most probable option between these three earthquake events, the PGA value of the earthquakes at the Mobarak Abad landslide was calculated. The magnitude is not the only factor for the destruction scale of an earthquake. Other driving factors include the distance of the earthquake to an area, the acceleration that the earthquake applies at a point, the lithology of the study area, and the fault causing the earthquake are effective. Among all of these impact factors, acceleration has the most significant effect on destruction. The dynamic force created by the fault decreases as it moves away from the epicenter due to passing through rocks with different materials, and the applied acceleration in a place far from the epicenter of an earthquake is less than the acceleration created by the earthquake. This acceleration is called PGA and can be determined by attenuation relations presented by many researchers. In this study, based on the data viability, two different attenuation relations of Zare *et al*. [49] and Ambraseys *et al*. [50] were used to calculate the value of PGA for the three remaining earthquakes, and finally, the values obtained from the two relationships were averaged. Table 6, besides the value of PGA, shows other characteristics of the three probable earthquakes.

Table 6. Characteristics of corresponding earthquakes of Mobarak Abad landslide.

	Year	Magnitude	Epicenter (km)	Latitude	Longitude	PGA (m/s^2)
1	743	7.2	57	35.3	52.2	0.15g
2	855	7.1	46.7	35.6	51.5	0.16g
3	1830	7.1	48.9	35.7	52.5	0.16g

Although the magnitude of the 743 AD earthquake is greater than the other two earthquakes, the value of PGA is the opposite. Finally, among these three earthquakes, based on the applied acceleration at the landslide, the 855 AD, and the 1830 AD earthquakes are slightly more probable than the 743 AD. Figure 12 shows the location of these three earthquakes relative to the Mobarak Abad landslide.

In addition, the mesoseismal area for the 1830 AD earthquake was extracted from 5 sources of Talebian *et al*. [51], Berberian [46], Ritz *et al*. [52], Solaymani Azad *et al*. [53], and Nazari *et al*. [54]. These mesoseismal areas were plotted in Figure 12, and they were compared to each other. The result depicts a good compatibility between these sources. Furthermore, the location of the 743 AD and the 855 AD earthquakes was only presented by Ritz *et al*. [52]. The comparison between the locations presented in this paper to the ones we presented in Figure 8, do not show any difference, and they were almost at the same point.

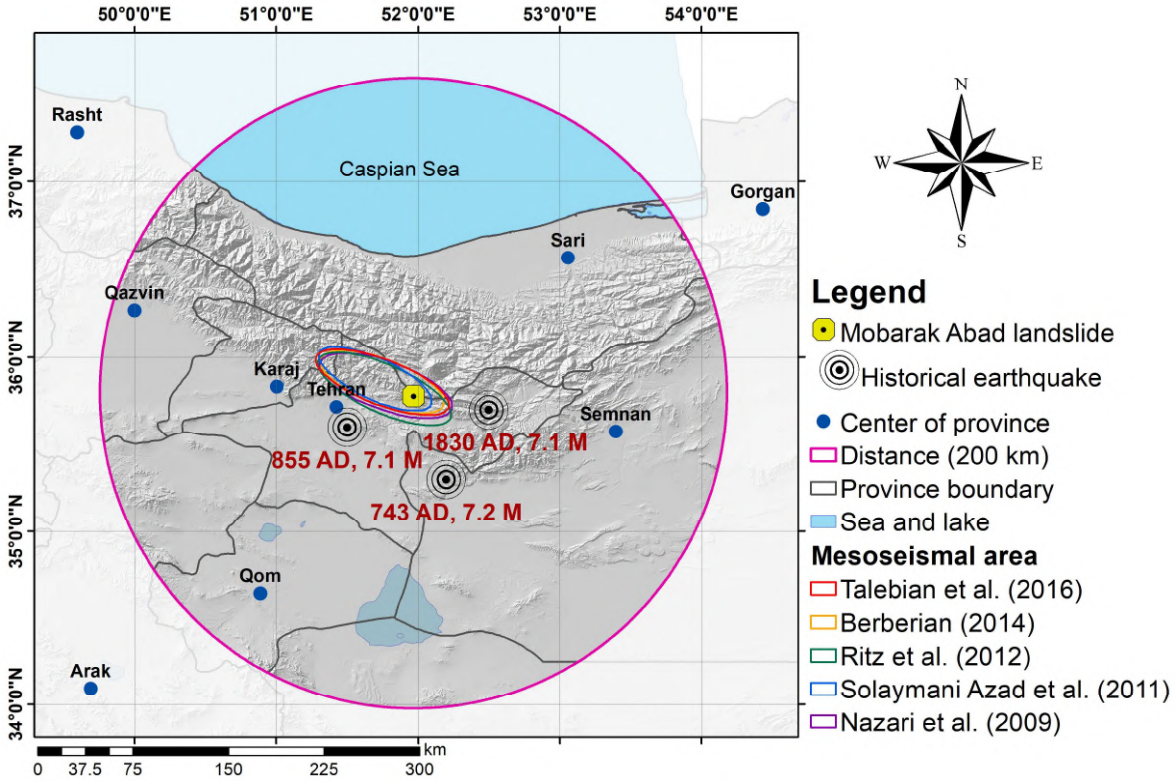

Figure 12. Location of the three probable earthquakes triggering the Mobarak Abad landslide.

5. Conclusions

Mobarak Abad landslide is a large yet active landslide that had been recorded in Mobarak formation. Due to the proximity to active faults such as Mosha, Khazar, and North Alborz, the idea arises that an earthquake causes the Mobarak Abad landslide. Therefore, with all the equations relating the geometry characteristics to volume, the average volume of the landslide was estimated to be 7469380.1 cubic meters, then, with the equations relating the area and volume of the landslide to magnitude, the corresponding earthquake's magnitude was measured between 5.4 and 7.2.

The corresponding earthquake was conducted by studying all the historical earthquakes within 200 kilometers of the landslide and removing the earthquakes whose magnitude was out of the mentioned range. This boundary condition was insufficient, so some other earthquakes were

eliminated using Keefer's graphs. In the next step, the maximum value of epicenter location error was considered for the remaining earthquakes, and the epicenter and hypocenter distances were updated. Finally, three earthquakes of 743 AD, 855 AD, and 1830 AD with magnitude of 7.2, 7.1, and 7.1 were left. These three earthquakes are the most responsible for triggering the Mobarak Abad landslide.

In the last stage, we also determined the value of PGA for these three earthquakes, and among them, two earthquakes of 855 AD and 1830 AD because of the more PGA compared to the 743 AD earthquake, identified more probable for being the corresponding earthquake of the Mobarak Abad landslide. Based on field investigation and engineering judgment of authors, and also several pieces of evidence have been observed such as scarps, cracks in different directions, and absence of smoothness, the 1830 AD earthquake is a more probable event which triggered the Mobarak Abad landslide. In addition, the current study leads to the improvement of the historical earthquake catalogue of Tehran by identifying the Mobarak Abad landslide as a site effect of the 1830 AD earthquake event.

References

[1]. Keefer, D. K. (1984). Landslides caused by earthquakes. *Geological Society of America Bulletin*, *95*(4), 406–421.

[2]. Highland, L., & Bobrowsky, P. T. (2008). *The landslide handbook: A guide to understanding landslides*. US Geological Survey Reston.

[3]. Komadja, G. C., Pradhan, S. P., Roul, A. R., Adebayo, B., Habinshuti, J. B., Glodji, L. A., & Onwualu, A. P. (2020). Assessment of stability of a Himalayan road cut slope with varying degrees of weathering: A finite-element-model-based approach. *Heliyon*, *6*(11), e05297.

[4]. Kadri, U. (2017). Tsunami mitigation by resonant triad interaction with acoustic–gravity waves. *Heliyon*, *3*(1), e00234.

[5]. Prasad, N. N. (1995). Landslides-Causes & Mitigation. *Centre for Water Resources Development, Kerala, India*, *21*, 48–54.

[6]. Wieczorek, G. F., Reid, M. E., Jodicke, W., Pearson, C., & Wilcox, G. (2007). Rainfall and Seasonal Movement of the Weeks Creek Landslide, San Mateo County, California. *US Geological Survey Data Series 278*.

[7]. Ling, S., Sun, C., Li, X., Ren, Y., Xu, J., & Huang, T. (2021). Characterizing the distribution pattern and geologic and geomorphic controls on earthquake-triggered landslide occurrence during the 2017 Ms 7.0 Jiuzhaigou earthquake, Sichuan, China. *Landslides*, *18*, 1275–1291.

[8]. Mahdavifar, M. R., Solaymani, S., & Jafari, M. K. (2006). Landslides triggered by the Avaj, Iran earthquake of June 22, 2002. *Engineering Geology*, *86*(2–3), 166–182.

[9]. Chen, C.-W., Sato, M., Yamada, R., Iida, T., Matsuda, M., & Chen, H. (2022). Modeling of earthquake-induced landslide distributions based on the active fault parameters. *Engineering Geology*, *303*, 106640.

[10]. Seed, H. B. (1969). Landslides during earthquakes due to soil liquefaction. *Journal of the Soil Mechanics and Foundations Division*, *95*(4), 1123–1123.

[11]. Qing-Zhao, Z., Qing, P., Ying, C., Ze-Jun, L., Zhen-Ming, S., & Yuan-Yuan, Z. (2019). Characteristics of landslide-debris flow accumulation in mountainous areas. *Heliyon*, *5*(9), e02463.

[12]. Chowdhury, R., Flentje, P., & Bhattacharya, G. (2009). *Geotechnical slope analysis*. CRC Press.

[13]. Stöcklin, J. (1974). Northern Iran: Alborz Mountains. *Geological Society, London, Special Publications*, *4*(1), 213–234.

[14]. Hessami, K., Jamali, F., & Tabassi, H. (2003). *Map of "Major Active Faults of Iran", International Institute of Earthquake Engineering (IIEES)* [Map]. International Institute of Earthquake Engineering (IIEES).

[15]. Ghayoumian, J. (2002). Seimareh Landslide, western Iran, one of the world's largest complex landslides. *Landslide News*, *13*, 23–27.

[16]. Shoaei, Z. (2014). Mechanism of the giant Seimareh Landslide, Iran, and the longevity of its landslide dams. *Environmental Earth Sciences*, *72*(7), 2411–2422.

[17]. Evans, S. G., Delaney, K. B., Hermanns, R. L., Strom, A., & Scarascia-Mugnozza, G. (2011). The formation and behaviour of natural and artificial rockslide dams; implications for engineering performance and hazard management. In *Natural and artificial rockslide dams* (pp. 1–75). Springer.

[18]. Sahbai, M., Chaichi, Z., & Nozari. (1997). *Map of "East of Tehran", Geological Survey and Mineral Exploration of Iran* [Map]. Geological Survey and Mineral Exploration of Iran.

[19]. Ehteshami-Moinabadi, M., & Nasiri, S. (2019). Geometrical and structural setting of landslide dams of the Central Alborz: A link between earthquakes and landslide damming. *Bulletin of Engineering Geology and the Environment*, *78*(1), 69–88.

[20]. Chen, Z., Zhang, B., Han, Y., Zuo, Z., & Zhang, X. (2014). Modeling accumulated volume of landslides using remote sensing and DTM data. *Remote Sensing*, *6*(2), 1514–1537.

[21]. Valkaniotis, S., Papathanassiou, G., & Ganas, A. (2018). Mapping an earthquake-induced landslide based on UAV imagery; case study of the 2015 Okeanos landslide, Lefkada, Greece. *Engineering Geology*, *245*, 141–152.

[22]. Guzzetti, F., Ardizzone, F., Cardinali, M., Rossi, M., & Valigi, D. (2009). Landslide volumes and landslide mobilization rates in Umbria, central Italy. *Earth and Planetary Science Letters*, *279*(3–4), 222–229.

[23]. Xu, C., Xu, X., Shen, L., Yao, Q., Tan, X., Kang, W., Ma, S., Wu, X., Cai, J., & Gao, M. (2016). Optimized volume models of earthquake-triggered landslides. *Scientific Reports*, *6*(1), 1–9.

[24]. Martin, Y., Rood, K., Schwab, J. W., & Church, M. (2002). Sediment transfer by shallow landsliding in the Queen Charlotte Islands, British Columbia. *Canadian Journal of Earth Sciences*, *39*(2), 189–205.

[25]. Abele, G. (1974). Bergstürze in den Alpen: Ihre Verbreitung, Morphologie und Folgeerscheinungen.

[26]. Whitehouse, I. E. (1983). Distribution of large rock avalanche deposits in the central Southern Alps, New Zealand. *New Zealand Journal of Geology and Geophysics*, *26*(3), 271–279.

[27]. Haflidason, H., Lien, R., Sejrup, H. P., Forsberg, C. F., & Bryn, P. (2005). The dating and morphometry of the Storegga Slide. *Marine and Petroleum Geology*, *22*(1–2), 123–136.

[28]. Ten Brink, U. S., Geist, E. L., & Andrews, B. D. (2006). Size distribution of submarine landslides and its implication to tsunami hazard in Puerto Rico. *Geophysical Research Letters*, *33*(11).

[29]. Guzzetti, F., Ardizzone, F., Cardinali, M., Galli, M., Reichenbach, P., & Rossi, M. (2008). Distribution of landslides in the Upper Tiber River basin, central Italy. *Geomorphology*, *96*(1–2), 105–122.

[30]. Fan, J., Li, X., Guo, F., & Guo, X. (2011). Empirical-statistical models based on remote sensing for estimating the volume of landslides induced by the Wenchuan earthquake. *Journal of Mountain Science*, *8*(5), 711–717.

[31]. Omidvar, E., & Kavian, A. (2011). Landslide Volume Estimation Based on Landslide Area in a Regional Scale (Case Study: Mazandaran Province). *Journal of Natural Environmental, Iranian Journal of Natural Resources*, *63*(4), 439–455. (In Persian)

[32]. Hadian-Amri, M., Solaimani, K., Kavian, A., Afzal, P., & Glade, T. (2014). Curve estimation modeling between area and volume of landslides in Tajan River basin, North of Iran. *Ecopersia*, *2*(3), 651–665.

[33]. Amirahmadi, A., Pourhashemi, S., Karami, M., & Akbari, E. (2016). Modeling of landslide volume estimation. *Open Geosciences*, *8*(1), 360–370.

[34]. Keefer, D. K., & Wilson, R. V. (1989). Prediction earthquakes-induce landslides, with emphasis on arid and semiarid environments (1989) Landslides in a semiarid environment, 2. *Riverside, California Inland Geological Society*, 118–149.

[35]. Keefer, D. K. (1994). The importance of earthquake-induced landslides to long-term slope erosion and slope-failure hazards in seismically active regions. In *Geomorphology and natural hazards* (pp. 265–284). Elsevier.

[36]. Hanks, T. C., & Kanamori, H. (1979). A moment magnitude scale. *Journal of Geophysical Research: Solid Earth*, *84*(B5), 2348–2350.

[37]. Hancox, G. T., Perrin, N. D., & Dellow, G. D. (2002). Recent studies of historical earthquake-induced landsliding, ground damage, and MM intensity in New Zealand. *Bulletin of the New Zealand Society for Earthquake Engineering*, *35*(2), 59–95.

[38]. Hancox, G. T., Dellow, G. D., & Perrin, N. D. (1997). Earthquake-induced landsliding in New Zealand and implications for MM intensity and seismic hazard assessment. Institute of Geological & Nuclear Sciences.

[39]. Malamud, B. D., Turcotte, D. L., Guzzetti, F., & Reichenbach, P. (2004). Landslides, earthquakes, and erosion. *Earth and Planetary Science Letters*, *229*(1–2), 45–59.

[40]. Nepop, R. K., & Agatova, A. R. (2008). Estimating magnitudes of prehistoric earthquakes from landslide data: First experience in southeastern Altai. *Russian Geology and Geophysics*, *49*(2), 144–151.

[41]. Agatova, A. R., & Nepop, R. K. (2011). Assessing the rate of seismogravitational denudation of the relief of southeastern Altai: The Chagan-Uzun R. Basin. *Journal of Volcanology and Seismology*, *5*(6), 421–430.

[42]. Xu, C., Xu, X., & Shyu, J. B. H. (2015). Database and spatial distribution of landslides triggered by the Lushan, China Mw 6.6 earthquake of 20 April 2013. *Geomorphology*, *248*, 77–92.

[43]. Nepop, R., & Agatova, A. (2016). Quantitative estimations of the Holocene erosion due to seismically induced landslides in the SE Altai (Russia) applying detailed profiling and statistical approaches. *International Journal of Georesources and Environment-IJGE (Formerly Int'l J of Geohazards and Environment)*, *2*(3), 104–118.

[44]. Ambraseys, N. N., & Melville, C. P. (1982). *A history of Persian earthquakes*. Cambridge University Press.

[45]. Berberian, M. (1994). *Natural hazards and the first earthquake catalogue of Iran.* International Institute of Earthquake Engineers and Seismology.

[46]. Berberian, M. (2014). Earthquakes and coseismic surface faulting on the Iranian Plateau (Vol. 17). Elsevier.

[47]. Shahvar, M. P., Zare, M., & Castellaro, S. (2013). A unified seismic catalog for the Iranian plateau (1900–2011). *Seismological Research Letters*, *84*(2), 233–249.

[48]. Ghafory-Ashtiani, M., & Mousavi, M. (2014). *Guideline for Seismic Hazard Analysis (No. 626)* (p. 43). Office of Deputy for Strategic Supervision, Department of Technical Affairs. (In Persian)

[49]. Zare, M., Ghafory-Ashtiany, M., & Bard, P.-Y. (1999). Attenuation law for the strong-motions in Iran. *Proceedings of the Third International Conference on Seismology and Earthquake Engineering*, *1*, 345–354.

[50]. Ambraseys, N. N., Douglas, J., Sarma, S. K., & Smit, P. M. (2005). Equations for the estimation of strong ground motions from shallow crustal earthquakes using data from Europe and the Middle East: Horizontal peak ground acceleration and spectral acceleration. *Bulletin of Earthquake Engineering*, *3*(1), 1–53.

[51]. Talebian, M., Copley, A. C., Fattahi, M., Ghorashi, M., Jackson, J. A., Nazari, H., Sloan, R. A., & Walker, R. T. (2016). Active faulting within a megacity: The geometry and slip rate of the Pardisan thrust in central Tehran, Iran. *Geophysical Supplements to the Monthly Notices of the Royal Astronomical Society*, *207*(3), 1688–1699.

[52]. Ritz, J.-F., Nazari, H., Balescu, S., Lamothe, M., Salamati, R., Ghassemi, A., Shafei, A., Ghorashi, M., & Saidi, A. (2012). Paleoearthquakes of the past 30,000 years along the North Tehran Fault (Iran). *Journal of Geophysical Research: Solid Earth*, *117*(B6).

[53]. Solaymani Azad, S., Ritz, J.-F., & Abbassi, M. R. (2011). Left-lateral active deformation along the Mosha–North Tehran fault system (Iran): Morphotectonics and paleoseismological investigations. *Tectonophysics*, *497*(1–4), 1–14.

[54]. Nazari, H., Ritz, J.-F., Salamati, R., Shafei, A., Ghassemi, A., Michelot, J.-L., Massault, M., & Ghorashi, M. (2009). Morphological and palaeoseismological analysis along the Taleghan fault (Central Alborz, Iran). *Geophysical Journal International*, *178*(2), 1028–1041.

شناسایی زلزله مسبب زمین‌لغزش مبارک‌آباد، شمال‌شرق تهران، ایران

عرفان امینی[1]، مسعود مجرب[2] و حسین معماریان[1*]

1. دانشکده مهندسی معدن، دانشکده فنی، دانشگاه تهران، تهران، ایران
2. شرکت مهندسین مشاور بنیان زمین پایدار، تهران، ایران

ارسال 2023/7/7، پذیرش 2023/09/01

* نویسنده مسئول مکاتبات: memarian@ut.ac.ir

چکیده:

به حرکت رو به پایین بخشی از مواد و مصالح زمین تحت تأثیر مستقیم نیروی گرانش، زمین‌لغزش گفته می‌شود. زمین‌لغزش‌ها توسط طیف گسترده‌ای از عوامل محرک نظیر زلزله‌ها و به‌عنوان اثر ساختگاهی آن رویداد می‌توانند ایجاد شوند. در مجاورت تهران زلزله‌های تاریخی قابل‌توجهی رخ‌داده است. بنابراین، ردیابی آنها می‌تواند کاتالوگ زلزله‌های تاریخی تهران را تقویت کند، زیرا تهران یک کلان‌شهر و پایتخت ایران است. هرچند که دیرینه‌لرزه‌شناسی نمی‌تواند بزرگا و ویژگی‌های لرزه‌ای زلزله‌های تاریخی را تعیین کند. زمین‌لغزش مبارک‌آباد، یک زمین‌لغزش بزرگ و تاریخی است که در جاده هراز، شریان حیاتی که تهران را به استان مازندران متصل می‌کند، واقع‌شده است و گسل‌های قابل‌توجهی مانند مشا، البرز شمالی و خزر در همسایگی آن وجود دارد. ازاین‌رو، این احتمال وجود دارد که این زمین لغزش توسط نیروی دینامیکی حاصل از یک زلزله رخ‌داده باشد. بنابراین در این تحقیق، ویژگی‌های هندسی زمین‌لغزش از طریق برداشت زمین‌شناسی اندازه‌گیری شدند. سپس با استفاده از روابط تجربی ارائه‌شده توسط محققین مختلف، به ترتیب حجم زمین‌لغزش و بزرگای زلزله مسبب تخمین زده شد. در ادامه، شعاع رومرکز و شعاع کانونی تمامی زلزله‌های تاریخی که در فاصله 200 کیلومتری از زمین‌لغزش بودند، مشخص شدند. سپس از تعدادی شرایط مانند نمودارهای کیفر، مقدار خطا در محل رومرکز زلزله و شتاب حداکثر روی سطح، برای حذف زلزله و شناسایی زلزله مسبب استفاده کردیم. نتایج نشان می‌دهد که دو زلزله 1830 و 855 میلادی با حداکثر شتاب 0/16g نسبت به زلزله 743 میلادی محتمل‌تر می‌باشند.

کلمات کلیدی: روابط تجربی، حجم زمین‌لغزش، بزرگا، شعاع رومرکز و شعاع کانونی، شتاب حداکثری زمین.